

• Original Paper •

Relative Impacts of Sea Ice Loss and Atmospheric Internal Variability on the Winter Arctic to East Asian Surface Air Temperature Based on Large-Ensemble Simulations with NorESM2[※]

Shengping HE^{*1,2,4}, Helge DRANGE¹, Tore FUREVIK^{2,1}, Huijun WANG^{3,4,5}, Ke FAN⁶,
Lise Seland GRAFF⁷, and Yvan J. ORSOLINI⁸

¹*Geophysical Institute, University of Bergen and Bjerknes Centre for Climate Research, Bergen 5020, Norway*

²*Nansen Environmental and Remote Sensing Center, Bergen 5007, Norway*

³*Key Laboratory of Meteorological Disaster, Ministry of Education/Joint International Research Laboratory of Climate and Environment Change (ILCEC)/Collaborative Innovation Center on Forecast and Evaluation of Meteorological Disasters (CIC-FEMD), Nanjing University of Information Science & Technology, Nanjing 211544, China*

⁴*Nansen-Zhu International Research Center, Institute of Atmospheric Physics, Chinese Academy of Sciences, Beijing 100029, China*

⁵*Southern Marine Science and Engineering Guangdong Laboratory (Zhuhai), Zhuhai 511458, China*

⁶*School of Atmospheric Science, Sun Yat-Sen University, and Southern Marine Science and Engineering Guangdong Laboratory (Zhuhai), Zhuhai 519082, China*

⁷*Norwegian Meteorological Institute, Oslo 0313, Norway*

⁸*Norwegian Institute for Air Research, Kjeller 2007, Norway*

(Received 10 January 2023; revised 23 May 2023; accepted 21 June 2023)

ABSTRACT

To quantify the relative contributions of Arctic sea ice and unforced atmospheric internal variability to the “warm Arctic, cold East Asia” (WACE) teleconnection, this study analyses three sets of large-ensemble simulations carried out by the Norwegian Earth System Model with a coupled atmosphere–land surface model, forced by seasonal sea ice conditions from preindustrial, present-day, and future periods. Each ensemble member within the same set uses the same forcing but with small perturbations to the atmospheric initial state. Hence, the difference between the present-day (or future) ensemble mean and the preindustrial ensemble mean provides the ice-loss-induced response, while the difference of the individual members within the present-day (or future) set is the effect of atmospheric internal variability. Results indicate that both present-day and future sea ice loss can force a negative phase of the Arctic Oscillation with a WACE pattern in winter. The magnitude of ice-induced Arctic warming is over four (ten) times larger than the ice-induced East Asian cooling in the present-day (future) experiment; the latter having a magnitude that is about 30% of the observed cooling. Sea ice loss contributes about 60% (80%) to the Arctic winter warming in the present-day (future) experiment. Atmospheric internal variability can also induce a WACE pattern with comparable magnitudes between the Arctic and East Asia. Ice-loss-induced East Asian cooling can easily be masked by atmospheric internal variability effects because random atmospheric internal variability may induce a larger magnitude warming. The observed WACE pattern occurs as a result of both Arctic sea ice loss and atmospheric internal variability, with the former dominating Arctic warming and the latter dominating East Asian cooling.

Key words: Arctic sea ice loss, warm Arctic–cold East Asia, atmospheric internal variability, large-ensemble simulation, NorESM2, PAMIP

Citation: He, S. P., H. Drange, T. Furevik, H. J. Wang, K. Fan, L. S. Graff, and Y. J. Orsolini, 2024: Relative impacts of sea ice loss and atmospheric internal variability on the winter Arctic to East Asian surface air temperature based on large-ensemble simulations with NorESM2. *Adv. Atmos. Sci.*, **41**(8), 1511–1526. <https://doi.org/10.1007/s00376-023-3006-9>.

※ This paper is a contribution to the special topic on Ocean, Sea Ice and Northern Hemisphere Climate: In Remembrance of Professor Yongqi GAO's Key Contributions.

* Corresponding author: Shengping HE
Email: Shengping.He@uib.no

Article Highlights:

- Both present-day and future Arctic sea-ice loss can force a negative winter Arctic Oscillation which exhibits a larger magnitude in the future case.
 - If only sea ice and atmospheric internal variability were considered, the former may contribute to more than 60% of winter Arctic warming.
 - Compared to Arctic sea ice loss, atmospheric internal variability could contribute to more than 70% of East Asian cooling.
 - A pattern of Arctic warming with a comparable magnitude of East Asian cooling is more likely induced by atmospheric internal variability.
-

1. Introduction

A robust finding in both observational and modeling studies covering the past few decades is the prominent near-surface warming in the Arctic coupled with dramatic declines in Arctic sea ice (Blunden and Arndt, 2012; Gao et al., 2015). Early studies have already acknowledged that the response of the Earth's surface temperature to an increasing air-borne fraction of carbon dioxide would heat the Earth and that the heating would be especially pronounced in polar regions (Arrhenius, 1896; Manabe and Stouffer, 1980). In contrast to the well-documented global and Arctic warming signals, a cooling trend with frequently occurring extreme cold winter spells is observed over Eurasia from the late-1990s to the early-2010s (Cohen et al., 2014; Francis et al., 2017; Coumou et al., 2018; Smith et al., 2022). The two winter temperature trends — Arctic warming and East Asian cooling — have initiated community-wide efforts to explore the possible linkages and the underlying dynamic and thermodynamic mechanisms between the two (Kim et al., 2014; Li et al., 2014; Francis and Vavrus, 2015; Kug et al., 2015; Cohen et al., 2020; Outten et al., 2023). Due to high albedo and effective blocking of the direct heat exchange between the atmosphere and the underlying ocean (He et al., 2018), Arctic sea ice and the snow on ice have been referred to as key factors for the observed Arctic near-surface warming (Serreze et al., 2007; Screen and Simmonds, 2010; Webster et al., 2018). Given that the meridional temperature gradient is a fundamental driver of the latitudinal position and intensity of the mid-latitude jet stream (Thompson and Wallace, 2001), Arctic warming and sea ice reduction can potentially induce changes in the atmospheric circulation and climate extremes at mid-latitudes (Cohen et al., 2012). Such an Arctic–mid-latitude linkage has been associated with abnormal cold and snowy winters over Eurasia in the 2000s (Cohen et al., 2013, 2014). Several mechanisms through which changes in the Arctic can be linked to changes at mid-latitudes have been proposed. Arctic warming can (1) decelerate the jet stream by weakening the low-level meridional temperature gradient (Francis, 2017); (2) intensify the Siberian high by stimulating downstream propagating Rossby waves (Honda et al., 2009; Li and Wang, 2013); (3) weaken the polar vortex or favor the negative phase of Arctic Oscillation by enhancing the upward propagation of planetary waves (Kim et al., 2014; Zhang et al., 2016, 2022; Xu et al.,

2019), and eventually influence the climate and weather at mid-latitudes (Cohen et al., 2014).

There is, however, no consensus as to whether the cooling trend and the frequent severe mid-latitude winters in the 1990s and 2000s are induced by Arctic changes (Gao et al., 2015; Francis, 2017; Cohen et al., 2020; Outten et al., 2023). Some studies have explicitly stated that there is a robust influence of Arctic sea ice loss on Eurasian winter temperature (Mori et al., 2014), while others claim that no such dynamic relationships exist (McCusker et al., 2016). Although a significant negative correlation has been found between the observational Arctic sea ice and Eurasian winter temperature (Outten and Esau, 2012), determining causality from such statistics is still an intractable problem (Smith et al., 2017). Furthermore, discrepancies among modeling results and between modeling and observational studies complicate the matter. For example, linkages between Arctic sea ice loss and more severe cold winters over Eurasia have been identified (Kim et al., 2014; Mori et al., 2019), whereas other studies have failed to find similar cold winter anomalies, cooling trends, or significant changes in extreme weather events in Eurasia (McCusker et al., 2016; Ogawa et al., 2018). Possible explanations for these discrepancies include deficiencies and diversities among climate models, detailed experimental designs (Screen et al., 2018), and the approaches used (England et al., 2022).

It is noteworthy that there is a consensus in the understanding of how Arctic sea-ice loss affects Arctic near-surface warming (Screen and Simmonds, 2010; Ogawa et al., 2018; Dai et al., 2019). However, the missing response of Eurasian cooling to Arctic sea ice loss inherent to many studies (McCusker et al., 2016; Ogawa et al., 2018) impedes the understanding of previously proposed pathways on the Arctic–mid-latitude climate linkages. A large intermodal spread in both the structure and the magnitude of climate response has been documented (He et al., 2020), and the underlying driving mechanisms are not well understood. One key factor in this respect is the signal-to-noise ratio. If the signal-to-noise ratio of some climate variables is low in models, the atmospheric internal variability can easily overwhelm the forced response to Arctic sea ice forcing (McCusker et al., 2016). Gao et al. (2015) have reviewed a large number of studies and found different and even contradictory conclusions on the impacts of Arctic sea ice loss. They suggest that the importance of atmospheric internal variability

should be further investigated, a comment that has been supported by observations from the last decade. For example, an abnormal Atlantic windstorm in January 2016 led to an Arctic warming beyond the 3.5 standard deviation level (Kim et al., 2017); meanwhile, an abnormal Ural blocking high resulted in a historical record-extreme cold spell in East Asia (Ma and Zhu, 2019). The roles of such abnormal atmospheric circulation regimes in impacting weather and, over time climate, in particular the extreme events, appear to become more evident (Zhang et al., 2021; Xu et al., 2022a, b). Due to the chaotic nature of the atmosphere and the interaction of processes on a range of temporal and spatial scales, it is challenging to isolate the effects of atmospheric internal variability from the effect of Arctic sea ice loss through statistical analysis of available observations. Gao et al. (2015) suggested that “coordinated multi-model ensemble experiments with identical sea ice and SST boundary conditions are needed to understand the associated mechanisms.”

The emergence of large ensembles of simulations provides a unique opportunity to identify and quantify the influence of internal climate variability. Here, internal climate variability is generally referred to as unforced climate variations intrinsic to a given climate state arising from atmospheric, oceanic, land, and cryospheric processes and their coupled interactions (Kay et al., 2015). To understand the effects of internal variations that arise from atmospheric (e.g., large-scale circulation patterns) and cryospheric (e.g., Arctic) processes, we will use large ensembles of simulations in which only the atmosphere and land components are coupled. All ensemble members have identical external forcings and identical boundary conditions of sea surface temperature (SST) and sea ice concentration (SIC), but with small perturbations in the atmospheric state at the start of the simulations. The differences between the ensemble mean of experiments with different SIC forcing can be interpreted as the response to the perturbed SIC, while the difference between individual ensemble members within the same model configuration is a measure of atmospheric internal variability. This protocol even allows us to assess the relative effects of sea ice loss and atmospheric internal variability which may reconcile the current divergent conclusions on the influence of Arctic sea ice on midlatitude climate (Cohen et al., 2020). Ideally, multi-member ensembles should be analyzed based on distinctly different model systems. Such a super-ensemble approach will reduce the impact of individual model system deficiencies, and thus highlight the leading — and presumably the govern-

ing — physical and dynamical processes and interactions involved. However, the presented analysis is limited to a single model system.

The remainder of this paper is organized as follows, section 2 describes the model and data, sections 3 and 4 present a discussion of the results, and section 5 provides a summary and conclusion.

2. Data and Methods

2.1. Observational data

The reanalysis data is the European Centre for Medium-Range Weather Forecasts (ECMWF) fifth-generation global atmospheric reanalysis (ERA5) (Hersbach et al., 2020). The Arctic sea ice extent index is derived from the National Snow and Ice Data Center (Fetterer et al., 2017). The linear trend has been removed from the observational dataset in the linear regression.

2.2. The Norwegian Earth System Model version 2 (NorESM2)

The model used in the presented analysis is the second version of the Norwegian Earth System Model (NorESM2) (Seland et al., 2020). The NorESM2 is based on the second version of the Community Earth System Model (CESM2) (Danabasoglu et al., 2020). The NorESM2 uses many components of the CESM2 and it shares the corresponding model code infrastructure. In contrast to CESM2, NorESM2 uses an isopycnic-coordinate oceanic general circulation model component, the Bergen Layered Ocean Model (Furevik et al., 2003), with an ocean-biogeochemistry module. Secondly, the NorESM2 has its own aerosol physics and chemistry module, an improved formulation for energy and momentum conservation, and an updated representation of deep convection and air-sea fluxes (Seland et al., 2020). It is an atmosphere-only, coarse-resolution (approximately $2^\circ \times 2^\circ$) version of the NorESM2, named NorESM2-LM, that is used in this study. Note that the experiments carried out for PAMIP with the CESM2 (not considered here) have a higher resolution ($1^\circ \times 1^\circ$).

2.3. Polar Amplification Model Intercomparison Project (PAMIP) simulations

The analyzed simulations follow the protocol of the Polar Amplification Model Intercomparison Project [PAMIP; (Smith et al., 2019)]. We used three sets of simula-

Table 1. Overview of the PAMIP simulations (run from 1 April 2000 to 31 May 2001). There is no interactive ocean while the atmosphere and land components are coupled.

Experiments	Different SIC conditions	No. of members
piArcSIC	a specific 30-year climatological SIC fields from the preindustrial control run*	100
pdSIC	present-day SIC fields from the observed 1979–2008 climatology*	200
futArcSIC	future SIC fields when global warming is $>2^\circ\text{C}$ than the preindustrial mean**	200

*“The preindustrial SIC field and future SIC fields” are derived from 31 CMIP5 models. More details can be found in Hausteijn et al. (2017) and Smith et al. (2019).

**“The present-day SST fields” are defined as the observed 1979–2008 climatology (Rayner et al., 2003).

tions that have the same radiative forcing (representing the year 2000) and the same SST fields (i.e., the 1979–2008 climatology from the Hadley Centre observational dataset (Rayner et al., 2003)). However, the three sets are forced with different SIC, namely the pre-industrial Arctic SIC, present-day SIC, and future Arctic SIC, respectively (referred to as piArcSIC, pdSIC, and futArcSIC; see Table 1). For the futArcSIC simulations, the Arctic SST is set to future values where the SIC differs by more than 10% between the future and preindustrial SIC fields (Screen et al., 2013; Peings et al., 2021). In the following developments, the sea ice edge is defined by an SIC of 15%. In all simulations, the sea-ice thickness is set to two meters in the Northern Hemisphere and one meter in the Southern Hemisphere in the PAMIP experiments.

The impacts of present-day (future) Arctic sea ice loss are represented as the differences between the ensemble-mean pdSIC (futArcSIC) simulations and those of piArcSIC. We focus on the boreal winter season (December, January, and February).

3. Arctic sea ice loss and its impacts in winter

Compared to the pre-industrial period, the present-day sea ice edge shows a clear poleward retreat in autumn and winter. The poleward retreat from November to the following February is largest in the Nordic Seas and the Barents-Kara Seas (Fig. 1a, contours). This change remains a major feature as the climate warms, with an even further poleward retreating sea ice edge (Fig. 1b, contours). However, in future winters, the retreating sea ice edge is mainly located in the Barents-Kara Seas and other regions are fully covered by sea ice. This means that there will still be substantial sea ice growth in winter even if the Arctic is nearly “ice-free” in summer (i.e., when the sea ice extent is less than 1×10^6 km²). As an

example, the present and future sea ice extents in February are similar throughout most of the Arctic, except for the Barents Sea. The month with the most dramatic sea ice decline is September which shows a 20%–30% decrease in the region from the Laptev to the Beaufort Seas at present, and a 60%–80% decrease is expected with an additional global warming of 2°C. Note also that the future November sea ice extent is even less than that of today's September extent.

The atmospheric response to present and future Arctic sea ice loss is diagnosed as the difference relative to the ensemble mean of piArcSIC. In the sensitivity experiments, higher SST is imposed where sea ice is significantly lost (see section 2.3). As a result, there is a local maxima of winter surface air temperature (SAT) warming in regions with substantial sea ice reduction. For the present-day climate, warming of more than 1.0°C occurs over the pan-Arctic region with a maximum of over 4.0°C in the Barents-Kara Seas (Fig. 2a). In the future climate, the pan-Arctic shows warming of over 2.0°C with a maximum of more than 6.0°C in the Barents-Kara and Bering-Chukchi Seas, and Hudson Bay (Fig. 2b). Note that the simulated Arctic warming might be underestimated in the future since the SST in the futArcSIC experiment is set to present-day values.

Interestingly, both the ensemble mean of pdSIC and futArcSIC show significant and similar cooling responses in East Asia (Figs. 2a, b). The tropospheric air temperature response to Arctic sea ice loss shows a robust vertical anomaly pattern — “warm Arctic, cold East Asia” — both in the present (Fig. 3a) and future (Fig. 3b) climates. The near-surface (pressure > 850 hPa) Arctic warming response to future sea ice loss is much stronger (>4.0°C; Fig. 3b, right panel) than that of the present-day sea ice loss with a maximum of about 1.5°C (Fig. 3a, right panel). The East Asian cooling response to future sea ice loss (Fig. 3b, left panel) is similar in magnitude compared to the present-day sit-

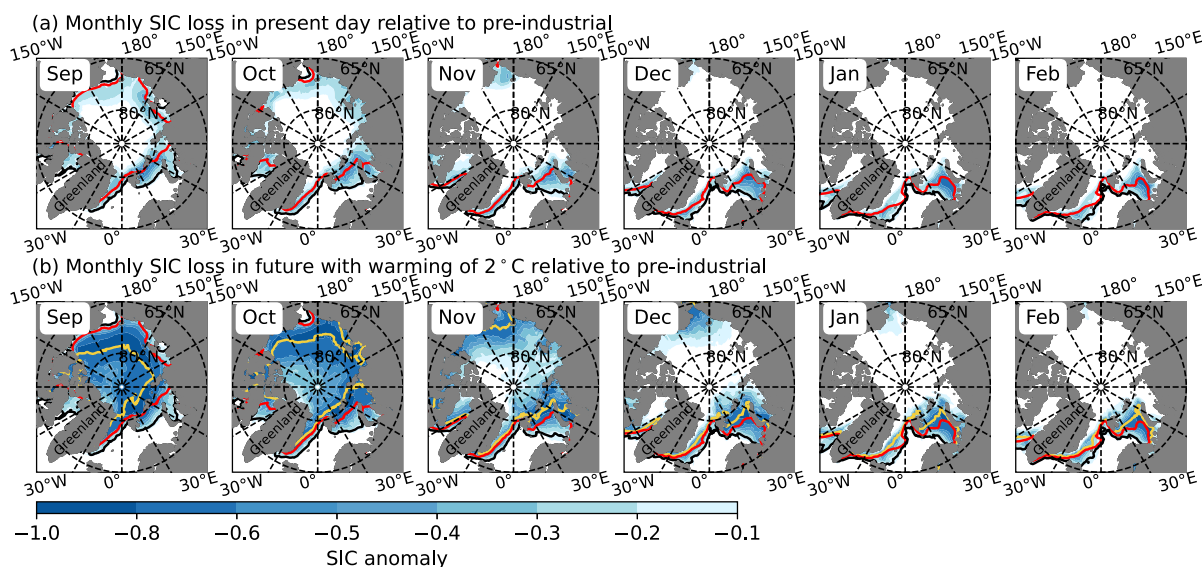


Fig. 1. Arctic sea ice loss as indicated by September to the subsequent February anomalies of the Arctic SIC for (a) the present-day and (b) future periods, respectively, relative to pre-industrial climatology. The black, red, and orange contours indicate the location of the mean sea ice edge in the pre-industrial, present-day, and future periods, respectively.

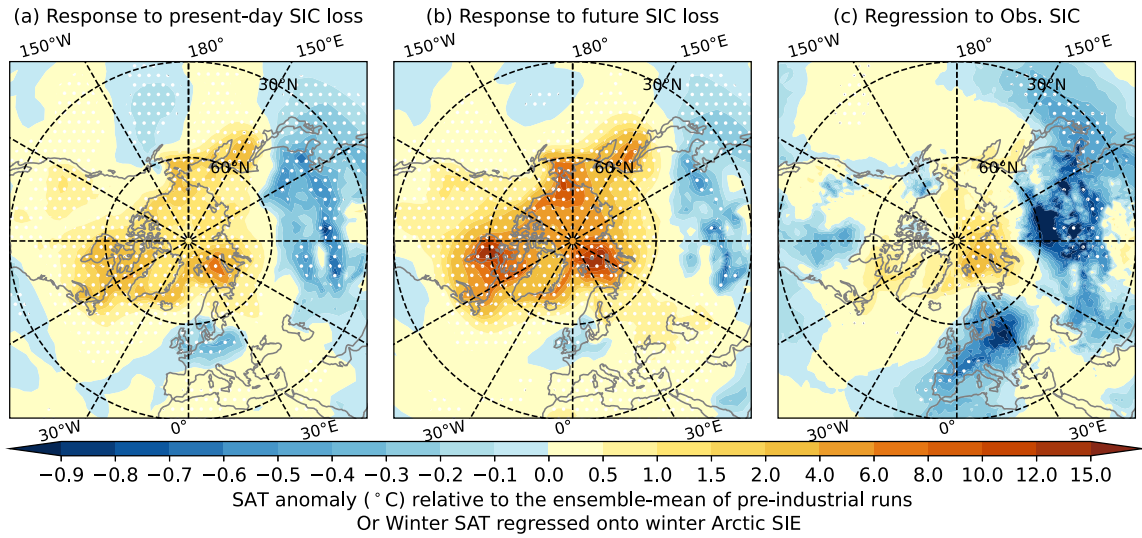


Fig. 2. Response of a “warm Arctic, cold East Asia” to Arctic sea ice loss as indicated by the ensemble response of winter surface air temperature (SAT; shading in °C; note the non-linear temperature scale) in (a) pdSIC and (b) futArcSIC, respectively, both relative to the ensemble-mean of pre-industrial runs. Panel (c) shows the regression of winter SAT (shading) onto the simultaneous Arctic sea ice extent index during 1979–2008 (to be consistent with the period of present-day forcing). Stippling indicates that anomalies are significant at the 95% confidence level.

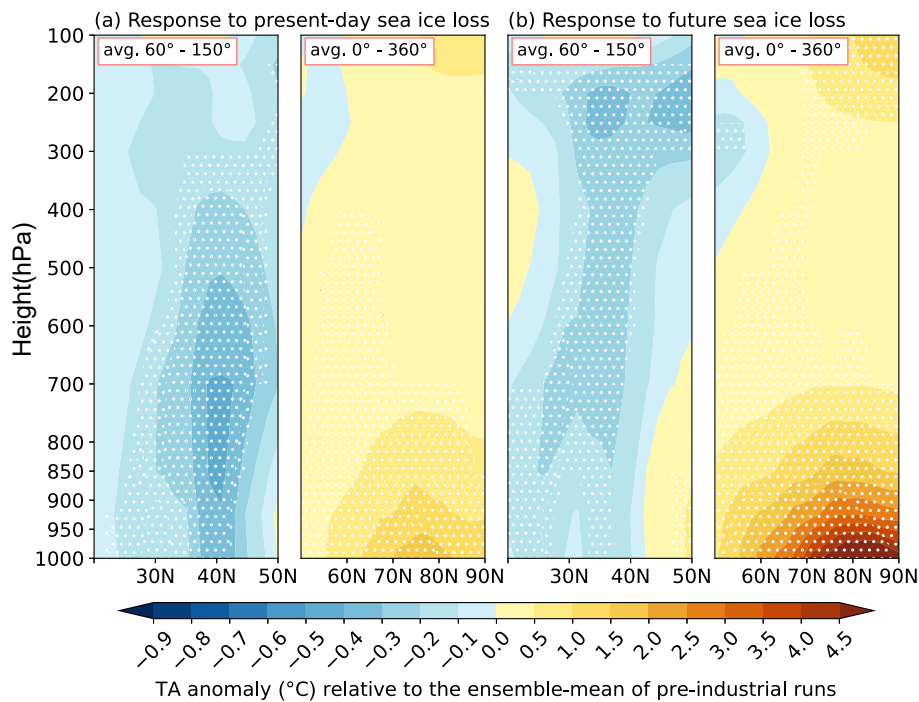


Fig. 3. Response of the winter tropospheric temperature to Arctic sea ice loss. Ensemble response of winter air temperature (TA; in °C) zonally averaged along 60°–150°E from 20°N to 50°N and zonally averaged along 0°–360° from 50°N to the North Pole in (a) pdSIC and (b) futArcSIC. Stippling indicates an ensemble mean response that is significant at the 95% confidence level.

uation (Fig. 3a, right panel), however, the latter has a stronger near-surface signature. This might be due to the limited remote effect of Arctic near-surface warming (He et al., 2020), and middle-tropospheric Arctic warming may play a dominant role in promoting the Arctic influences on the East Asian winter climate (Xu et al., 2019; Labe et al.,

2020).

The similar East Asian cooling response may be due to the similar spatial distribution of Arctic sea ice in winter (especially in January and February, see Figs. 1a, b). However, it should be noted that the magnitude of the East Asian cooling response (about -0.3°C) is less than 20% of the simu-

lated Arctic warming and it is only about 30% of its statistically estimated observation-based counterpart (Fig. 2c). This finding is consistent with Blackport and Screen (2021) who concluded that observed statistical connections may overestimate the causal effects of Arctic sea ice changes on mid-latitude winter climate.

The large difference between the modeled and observational-based analysis has been a major source of current debates on whether Arctic climate change can physically influence the mid-latitude winter climate (Mori et al., 2019; Cohen et al., 2020; Zappa et al., 2021). The results presented here confirm that Arctic sea ice loss has a robust—albeit rather weak—influence on East Asian winter cooling. The obtained cooling effect can be easily offset by other factors, in which internal atmospheric variation is a key candidate (see section 4). As shown in Fig. 4, if 50 ensemble members are randomly chosen 100 times from the large-ensemble simu-

lations (total of 200 members), the East Asian winter cooling in the 50 random ensemble-mean realizations can range from -0.41°C to -0.04°C in pdSIC (Fig. 4a), and from -0.28°C to $+0.05^{\circ}\text{C}$ in futArcSIC (Fig. 4b).

Since the only difference in the experimental design of the ensemble members is perturbations to the atmospheric initial state, the range of East Asian winter cooling among the 100 different 50 (or 100)-random-member ensemble mean (Fig. 4) can be attributed to atmospheric internal variability. It is noteworthy that the smaller the number of random members, the larger the range of the East Asian winter response, and the higher the probability that the East Asia region will show a warming response. This problematic phenomenon has been pointed out by Peings et al. (2021) that “100-member ensembles are still significantly influenced by internal variability, which can mislead conclusions”.

When the number of random members is increased to

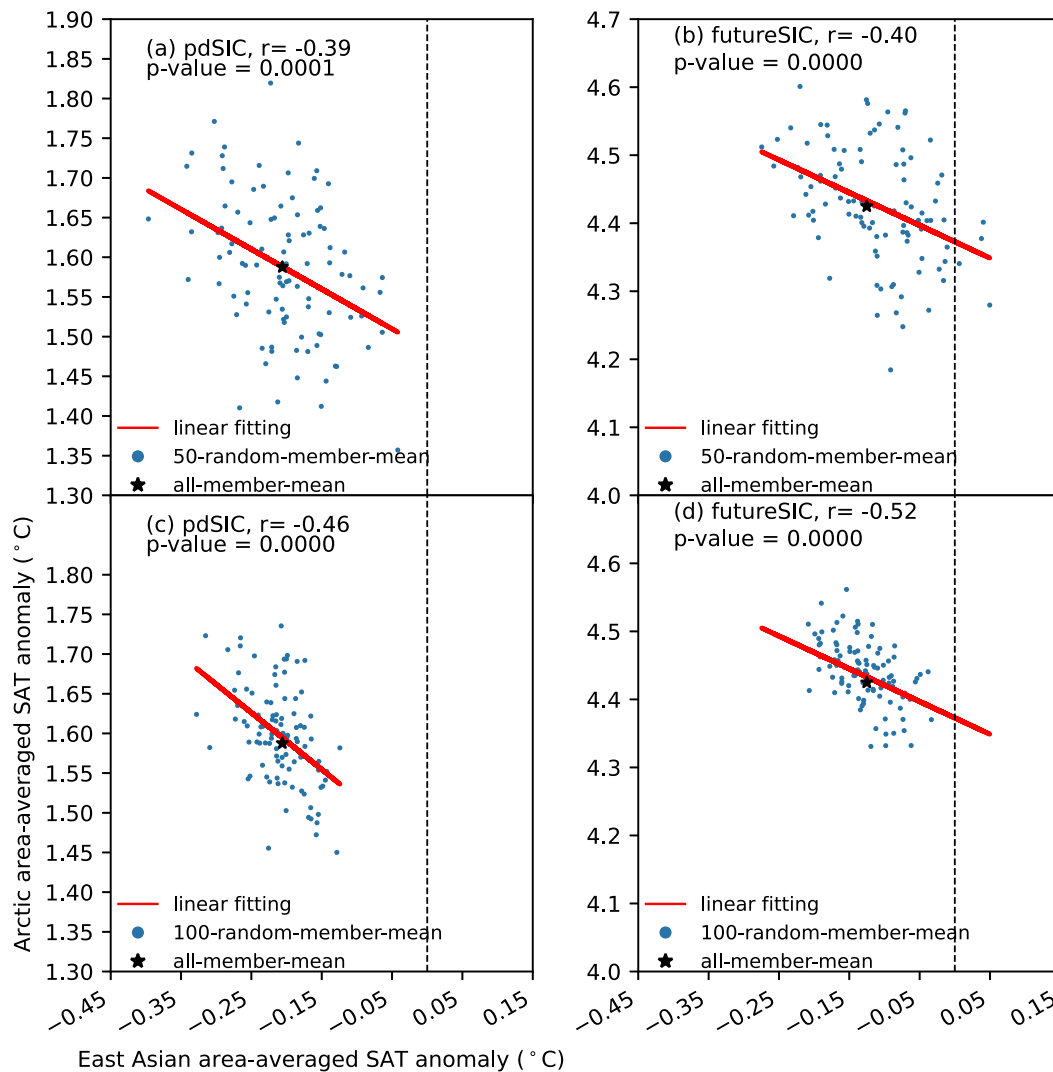


Fig. 4. Weak impacts of Arctic sea ice loss on warm Arctic–cold East Asia as demonstrated from scatterplots of winter SAT anomalies (in $^{\circ}\text{C}$; relative to the ensemble mean of piArcSIC) between the area-averaged Arctic (north of 65°N) and the area-averaged East Asian (25° – 45°N , 80° – 150°E) SAT anomalies among the 100 different 50-random-member ensemble mean for (a) pdSIC and (b) futArcSIC. To better reflect their differences, the y-axes in (a) and (b) have the same scale. The star indicates the results of all-member-mean.

100, the East Asian winter temperature shows a robust cooling response (i.e., no warming) to Arctic sea ice loss both for present-day and future climates (Figs. 4c, d). This indicates that ensembles on the order of tens of realizations, may have contributed to divergent conclusions in past studies. For example, the ensemble members in many previous studies range from 20 to 50 (Gao et al., 2015; Ogawa et al., 2018). On the other hand, even though the atmospheric internal variability has led to different magnitudes of SAT anomalies, a significant negative relationship (correlation of about -0.4) is obtained between the Arctic and the East Asian SAT anomalies (Fig. 4). This indicates that some underlying atmospheric circulation patterns may be actively involved (see section 4).

In both pdSIC and futArcSIC, the atmospheric circulation responses to Arctic sea ice loss are a high-pressure ridge extending from Greenland to Siberia, and low-pressure anomalies in the North Atlantic and North Pacific (Figs. 5a, b; shading). These anomalies resemble the negative phase of the North Atlantic Oscillation (NAO) and a strengthened Siberian high. In the mid-troposphere, the 500-hPa geopotential heights show positive anomalies over the Arctic with negative anomalies in the North Atlantic and North Pacific (Figs. 5a, b; contours), producing a response that projects onto a negative phase of the Arctic Oscillation. These large-scale atmospheric circulation responses have been reported in previous studies (Liu et al., 2012; Smith et al., 2022). It is noteworthy that the magnitude of height anomalies in futArcSIC (Fig. 5b) is larger than that in the pdSIC (Fig. 5a), implying a stronger future impact of additional sea ice loss on the

large-scale atmospheric circulation. However, the winter cooling over East Asia in the futArcSIC (Fig. 2b) is weaker than that in the pdSIC (Fig. 2a). This weakened cooling response may be attributed to the stronger Arctic warming in the futArcSIC (Fig. 2b) which may lead to weaker cold advection to East Asia even though there are stronger circulation anomalies.

However, it should be emphasized that the simulated atmospheric response is not fully consistent with the observed patterns. First, the observed Siberian high anomaly is stronger and with a larger spatial extent (Fig. 5c, shading). Secondly, the major center of the observed positive anomaly of 500-hPa geopotential height is located over the Ural region, and the negative anomalies in the North Atlantic and the North Pacific extend deeper into the Eurasian continent (Fig. 5c, contours), indicating a more intensified Ural blocking, Siberian high, and East Asian trough. As a result, the observation-based analysis shows a stronger cooling anomaly (about -0.8°C) in East Asia (Fig. 2c). At the same time, there is significant warming centered in the Barents-Kara Seas region with a magnitude of about four times that of the East Asian cooling. The dominant differences between the simulated and observed large-scale atmospheric circulation anomalies (Fig. 5) imply that there may be some other factors contributing to a “warm Arctic, cold East Asia”, for instance, atmospheric internal variability. In the absence of known fingerprint patterns (Hasselmann, 1997), the relative contributions of the two are, in general, impossible to identify utilizing observational analysis. Large-ensemble simulations can address this challenge, which will be dis-

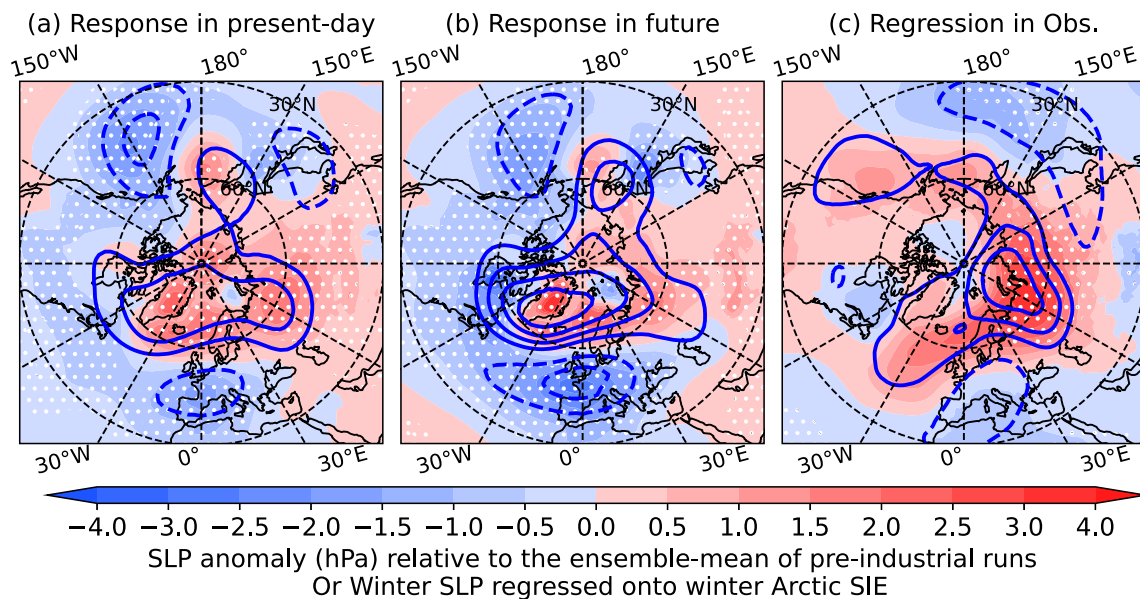


Fig. 5. Response of a negative Arctic Oscillation to Arctic sea ice loss as indicated by the ensemble response of winter sea level pressure (SLP, shading, units: hPa) and 500-hPa geopotential height (H500, contours, units: gpm) in (a) pdSIC and (b) futArcSIC. Panel (c) shows the regression of SLP (shading) and H500 (contours), respectively, in winter onto the simultaneous Arctic sea ice extent index during 1979–2008 (to be consistent with the period of present-day forcing). Stippling indicates where the anomaly is significant at the 95% confidence level. The contour interval is 10 gpm.

cussed in the next section.

4. Relative contribution of Arctic sea ice loss and atmospheric internal variability

From winter SAT reanalysis, the northern hemisphere shows the largest interannual variations at mid and high latitudes, in particular in the region extending from northern Europe to Siberia, over northern North America, and where the sea ice edge fluctuates, i.e., the Barents-Kara and Beaufort-Bering Seas (Fig. 6a). These variations are mainly caused by internal climate variations arising from atmospheric, oceanic, land, and cryospheric processes and their coupled interactions (Kay et al., 2015).

Based on the above considerations, the standard deviation (STD) of the large-ensemble members can be viewed, at least in part, as a measure of atmospheric internal variations because the only difference in experiment design among these members is a small atmospheric initial condition. The spatial distribution of the STD of winter SAT in both pdSIC (Fig. 6b) and futArcSIC (Fig. 6c) shows an overall correspondence to its observational-based counterpart (Fig. 6a). Furthermore, the magnitude of the simulated STD over the continents is close to that of the reanalysis. In contrast, the STD of the simulated winter SAT over the Arctic Ocean is, in general, well below that in the reanalysis. For example, in the Barents Sea, the simulated STD is less than 30% of the observational-based value. This indicates that the effects of atmospheric internal variability at the mid-latitudes are stronger than that in the Arctic; further noting that the atmospheric internal variability at mid-latitudes does not significantly differ between pdSIC and futArcSIC.

To identify the pattern and magnitude of the relative effect of sea ice loss and atmospheric internal variability in futArcSIC, the following approach has been adopted.

The contribution from future Arctic sea ice loss is estimated as the difference between the ensemble-mean fields (e.g., SAT, SLP, Z500) of futArcSIC and piArcSIC (the former minus the latter). In reference to Fig. 2b, for every grid point, the SAT anomaly can be referred to as ΔSAT . The contribution of atmospheric internal variability in futArcSIC is estimated as the STD of the 200 ensemble members of futArcSIC (Fig. 6c). The SAT anomaly induced by atmospheric internal variability is referred to as STD_{SAT} .

Ideally, the total variance of the simulated winter SAT, which is induced by both Arctic sea ice loss and atmospheric internal variability, can then be estimated as the sum of STD_{SAT} and ΔSAT when ΔSAT is positive, or the sum of $-\text{STD}_{\text{SAT}}$ and ΔSAT when ΔSAT is negative. Note that, the sign of ΔSAT is considered to take into account the sign of the “warm Arctic, cold East Asia” pattern (see Figs. 2a, b).

Correspondingly, the relative contribution of future Arctic sea ice loss (units: %) is then given by the ratio between the sea ice-induced winter SAT and the total variance of simulated winter SAT:

$$\Delta\text{SAT}/(\Delta\text{SAT} + \text{sign}(\Delta\text{SAT}) \times \text{STD}_{\text{SAT}}) \times 100,$$

where $\text{sign}(\Delta\text{SAT})$ is the sign of ΔSAT . The resulting field is shown in Fig. 7b. The residual can be attributed to the atmospheric internal variability. Applying the above procedure to the pdArcSIC, we can estimate the relative (percentage) contribution of present-day Arctic sea ice loss as shown in Fig. 7a.

The Arctic sea ice loss has the largest impact on the winter SAT variations in the regions of the Barents-Kara Seas, Sea of Okhotsk, Hudson Bay, the Bering-Chukchi Seas, and the Labrador Sea, with the maximum contribution exceeding 50% for pdSIC (Fig. 7a) and over 70% for futArcSIC (Fig. 7b). Meanwhile, the Arctic sea ice loss may have a cool-

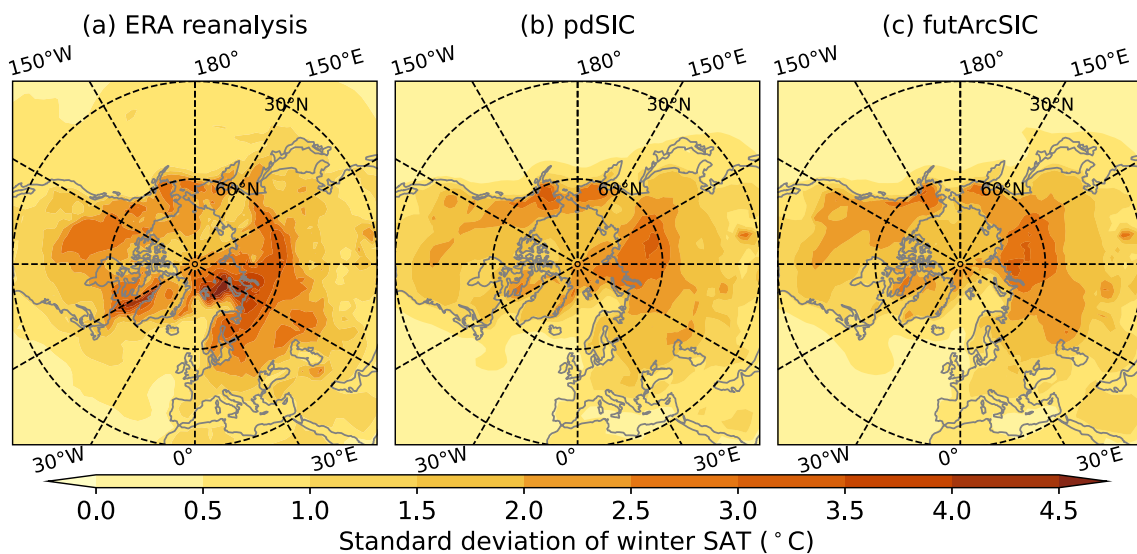


Fig. 6. Atmospheric internal variability of winter SAT as evidenced by (a) the standard deviation (STD, units: °C) of winter SAT during 1979–2008 (to be consistent with the period of present-day forcing) in the ERA5; and (b) and (c) which show the STD of winter SAT among 200 individual members of pdSIC and futArcSIC, respectively.

ing effect on the winter SAT in East Asia (Figs. 2a, b) but the contribution is less than 30% of the statistical estimation based on the observed Arctic sea ice loss (i.e., Fig. 2c). This quantitative estimation, obtained here from atmosphere-only simulations, is similar to that from coupled case-study simulations of the 2007 sea ice loss in Orsolini et al. (2012), who found the largest sea ice-induced surface temperature impact to be located over the Arctic and, to a lesser extent, along the Pacific coast of Asia. Furthermore, there are only small differences between the present-day and future SAT response over East Asia (Fig. 7). In other words, the contribu-

tion of atmospheric internal variability to Arctic SAT variability is less than 50% in the present climate and will decrease as the Arctic sea ice continues to shrink in the future (due to more open water in winter). In contrast, about 60% of the variance of winter SAT in East Asia is robustly dominated by atmospheric internal variability.

To check whether specific atmospheric circulation patterns are involved in the case of anomalously positive Arctic SAT anomalies, we choose some special ensemble members from the pdSIC (futArcSIC) experiments; in these members, the Arctic area-averaged SAT is higher by one STD

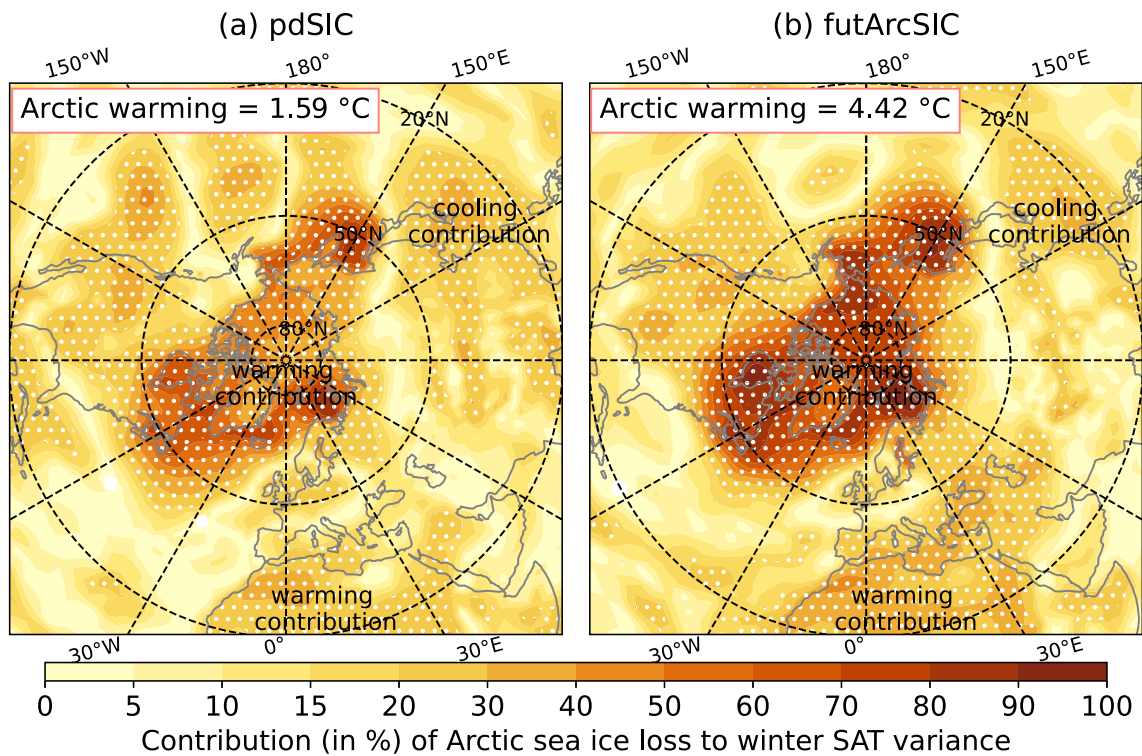


Fig. 7. Contribution of Arctic sea ice loss to winter SAT variance in (a) pdSIC and (b) futArcSIC. Stippling indicates where the contribution is significant at the 95% confidence level. The text “warming contribution” and “cooling contribution” refers to the large-scale positive and negative SAT anomalies shown in Figs. 2a and 2b.

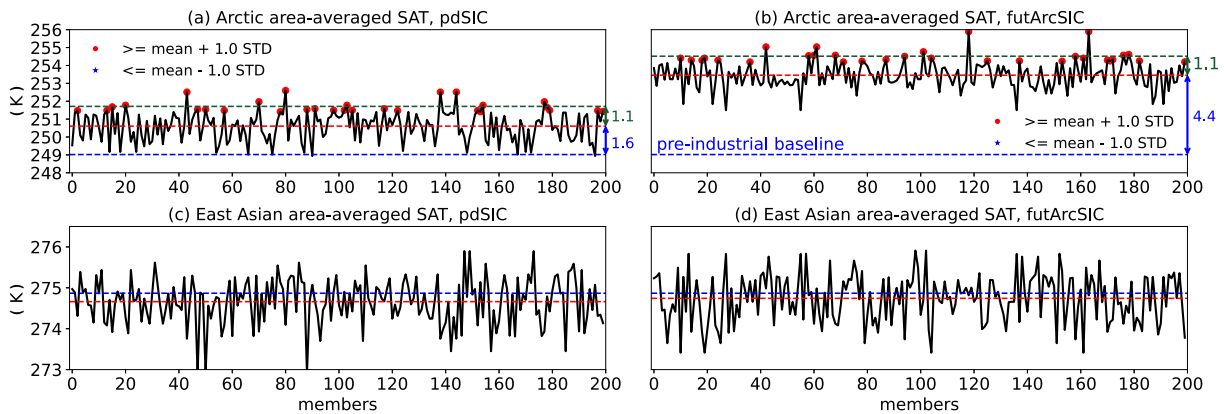


Fig. 8. Atmospheric internal variability evidenced by Arctic area-averaged winter SAT (65° – 90° N, 0° – 360°) of all members in (a) pdSIC and (b) futArcSIC. The red dots indicate the special members whose temperatures are higher than the all-ensemble mean (the red dashed lines) by one STD; the blue dashed lines show the ensemble mean of piArcSIC; and the green dashed lines show the ensemble mean of these special warm (red-colored) members. Panels (c) and (d) are the same as in (a) and (b), but for the East Asian area-averaged winter SAT.

compared to the 200-member ensemble mean of pdSIC (futArcSIC). As shown in Figs. 8a, d, This criterion yields 29 and 31 members in pdSIC and futArcSIC, respectively. The Arctic area-averaged winter SAT in the ensemble mean of these 29 (31) members is about 1.1°C higher than the 200-member ensemble mean of pdSIC (futArcSIC) which, at the same time, is about 1.6°C (4.4°C) above the ensemble mean of piArcSIC. Quantitatively, ignoring the effects of other external forcing and other boundary forcing, the present-day Arctic sea ice loss may have contributed to about 60% (i.e., $1.6/(1.1 + 1.6)$, see Fig. 8a) of the winter Arctic near-surface warming, increasing to about 80% [i.e., $4.4/(4.4 + 1.4)$, see Fig. 8b) in a future climate (also see Fig. 7 and Eq. (1)).

The pattern and magnitude of the difference between the members with the warmest Arctic in pdSIC (or futArcSIC) and the ensemble mean of the full set of members in pdSIC (or futArcSIC) are displayed in Fig. 9, resembling the so-called “warm Arctic–cold East Asia” pattern (Kug et al., 2015). The positive SAT anomalies in the Arctic and the negative anomalies further south are comparable in magnitude (i.e., the negative and positive SAT anomalies in Fig. 9 have similar scale), and they are consistent with an atmospheric dynamic effect (Luo et al., 2016) (see their Fig. 8a). The negative SAT anomalies caused by the atmospheric internal variability can exceed -1.0°C (Fig. 9). This cooling effect is about three times larger than that induced by Arctic sea ice loss (Figs. 2a, b), confirming a strong impact of atmo-

spheric internal variability on mid-latitude winter SAT. Note that the opposite effect (i.e., warming effect) on the East Asian winter SAT may also be induced by atmospheric internal variability. This implies that East Asian cooling caused by Arctic sea ice loss can be overwhelmed by internal atmospheric variations. In contrast, the Arctic warming caused by sea ice loss may not be overwhelmed by atmospheric internal variability, especially when the Arctic sea ice has decreased more dramatically. For example, the internally-induced Arctic winter SAT anomalies in the futArcSIC simulations are about 1.5°C to 2.0°C (Fig. 9b), which are smaller than those induced by the future Arctic sea ice loss of about 4.0 to 6.0°C (Fig. 2b).

The large-scale atmospheric circulation (Fig. 10) associated with the internally-induced “warm Arctic–cold East Asia” pattern (Fig. 9) is different from the ice-induced pattern (Figs. 4a, b). The former is characterized by a high-pressure ridge extending from the Ural mountains and eastward in Siberia, with regions of anomalous low pressure located in the North Atlantic and North Pacific Oceans (Fig. 10, shading). The corresponding 500-hPa geopotential height anomalies indicate an intensified Ural blocking and a deepened East Asian trough (Fig. 10, contours). The spatial distribution resembles the observational counterpart that is linearly regressed onto the winter Arctic sea ice extent (Fig. 5c). Thus, the observed, statistical relationship between the Arctic sea ice and the mid-latitude winter climate mainly reflects

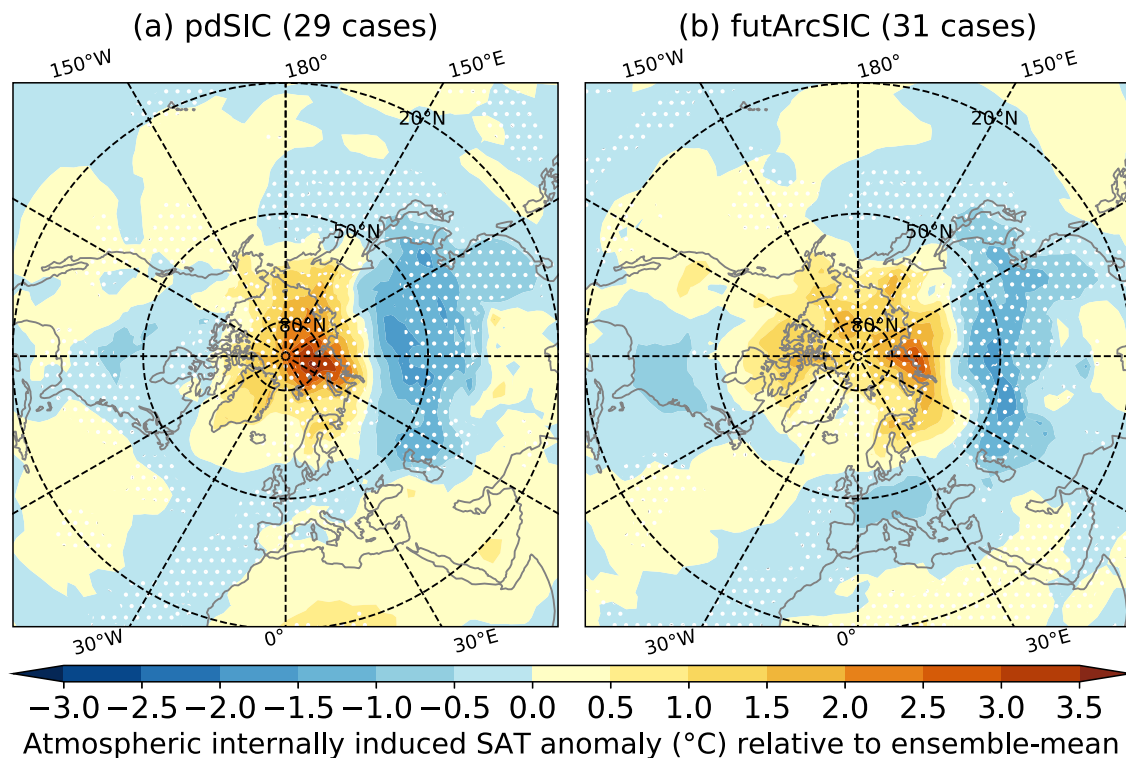


Fig. 9. Impacts of atmospheric internal variability on warm Arctic–cold East Asia as evidenced by the winter SAT anomalies (shading, units: $^{\circ}\text{C}$) of special members with extreme Arctic warming (shown by red dots in Fig. 8) in (a) pdSIC and (b) futArcSIC. Anomalies are the differences between the ensemble mean of these warm members in pdSIC (futArcSIC) and the full 200-member ensemble mean of the pdSIC (futArcSIC). Stippling indicates anomalies significant at the 95% confidence level.

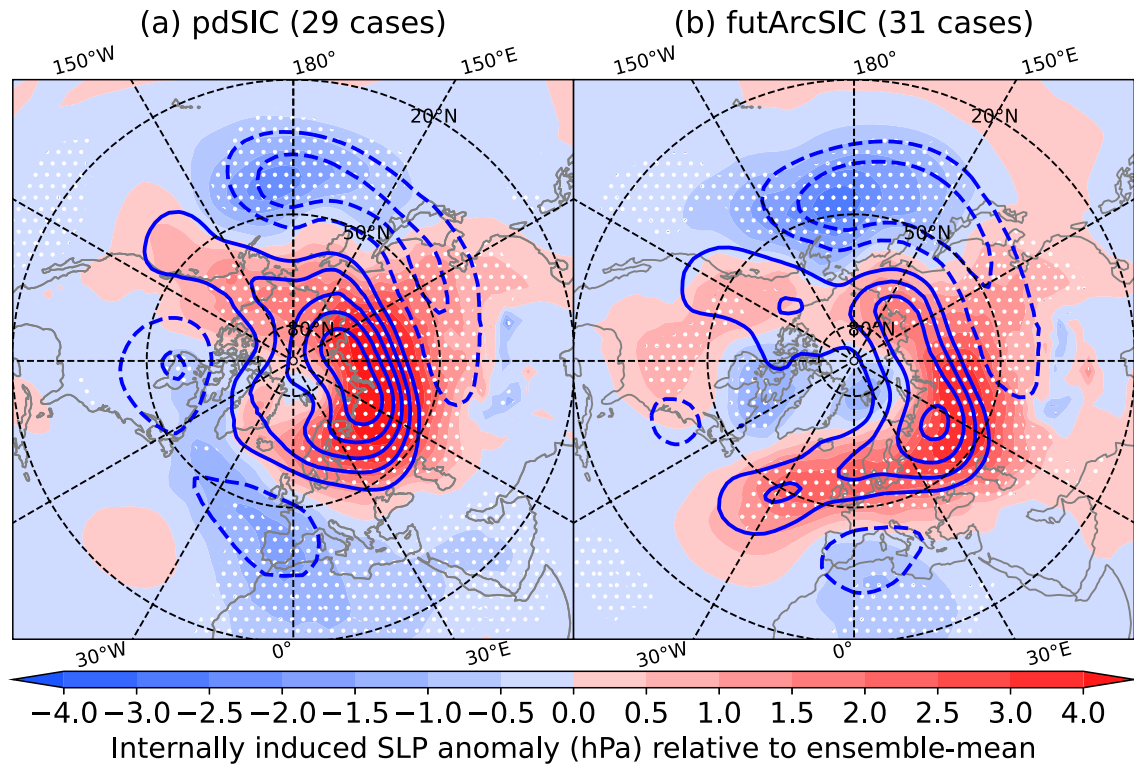


Fig. 10. Atmospheric circulation related to the internally-induced Arctic warming is displayed as in Fig. 9 but applied to the variables SLP (shading, units: hPa) and H500 (contours; interval is 10 gpm). Stippling indicates that the anomalies are significant at the 95% confidence level.

atmospheric dynamics. This is consistent with the results of Blackport and Screen (2021).

By combining the effects of Arctic sea ice loss and the atmospheric internal variability as displayed in Fig. 11, the atmospheric circulation response consists of a distorted anticyclonic anomaly at high latitudes and a cyclonic anomaly at lower latitudes extending across the North Pacific to East Asia, especially at 500 hPa, displaying a negative phase of AO with intensified Ural blocking (Figs. 11c, d). The “warm Arctic–cold East Asia” pattern in the simulations is more consistent with the observed characteristics (Fig. 5c) — the magnitude of Arctic warming is much larger (about four times) than that of the East Asian cooling (Figs. 11a, b). This strongly indicates that the observed “warm Arctic–cold East Asia” pattern is a result of both Arctic sea ice loss and atmospheric internal variability, where sea ice loss is the dominant factor for the Arctic warming while atmospheric internal variability is the dominant factor for the East Asian cooling.

5. Conclusions

Arctic sea ice is a key factor in causing the Arctic near-surface warming. In the atmosphere, there is an intrinsic co-variability between the Arctic and East Asian winter SAT. Therefore, based on the observational datasets, the scientific community has found many significant relationships between the Arctic sea ice, Arctic warming, the Siberian

high, and East Asian cooling. Due to the close interaction and feedback within the climate system, it has been challenging to robustly quantify the causal or driving effects of Arctic sea ice from only about 40 years of sea ice observations. Especially, when the fast-changing and chaotic atmosphere introduces additional difficulty in identifying any signal against naturally occurring variations. To quantitatively estimate the relative impacts of Arctic sea ice loss and atmospheric internal variability on winter SAT variations in the Arctic and in East Asia, this study uses three sets of large-ensemble simulations by the NorESM2-LM following the PAMIP protocol (Smith et al., 2019). These simulations are specifically designed to assess the effects of Arctic sea ice loss and internal variability.

The geographic regions of strong Arctic warming are closely related to the retreat of sea ice. The simulated Arctic warming is much larger than the magnitude of the East Asia cooling response, and the latter is about 30% of the observation-based, statistical estimate (Figs. 2a and 2b vs. 2c). Arctic sea ice loss can robustly force a negative phase of the Arctic Oscillation with a zonally symmetric structure, accompanied by an intensified Siberian high (Figs. 5a, b). This finding is in line with previous modeling studies (Liu et al., 2012) (see their Fig. 4c). The simulated atmospheric pattern has some resemblance to the observed pattern associated with the observed Arctic winter sea ice loss, for instance, the intensified Siberia high (Fig. 5c). On the other hand, the observational counterpart does not have a zonally symmetric structure

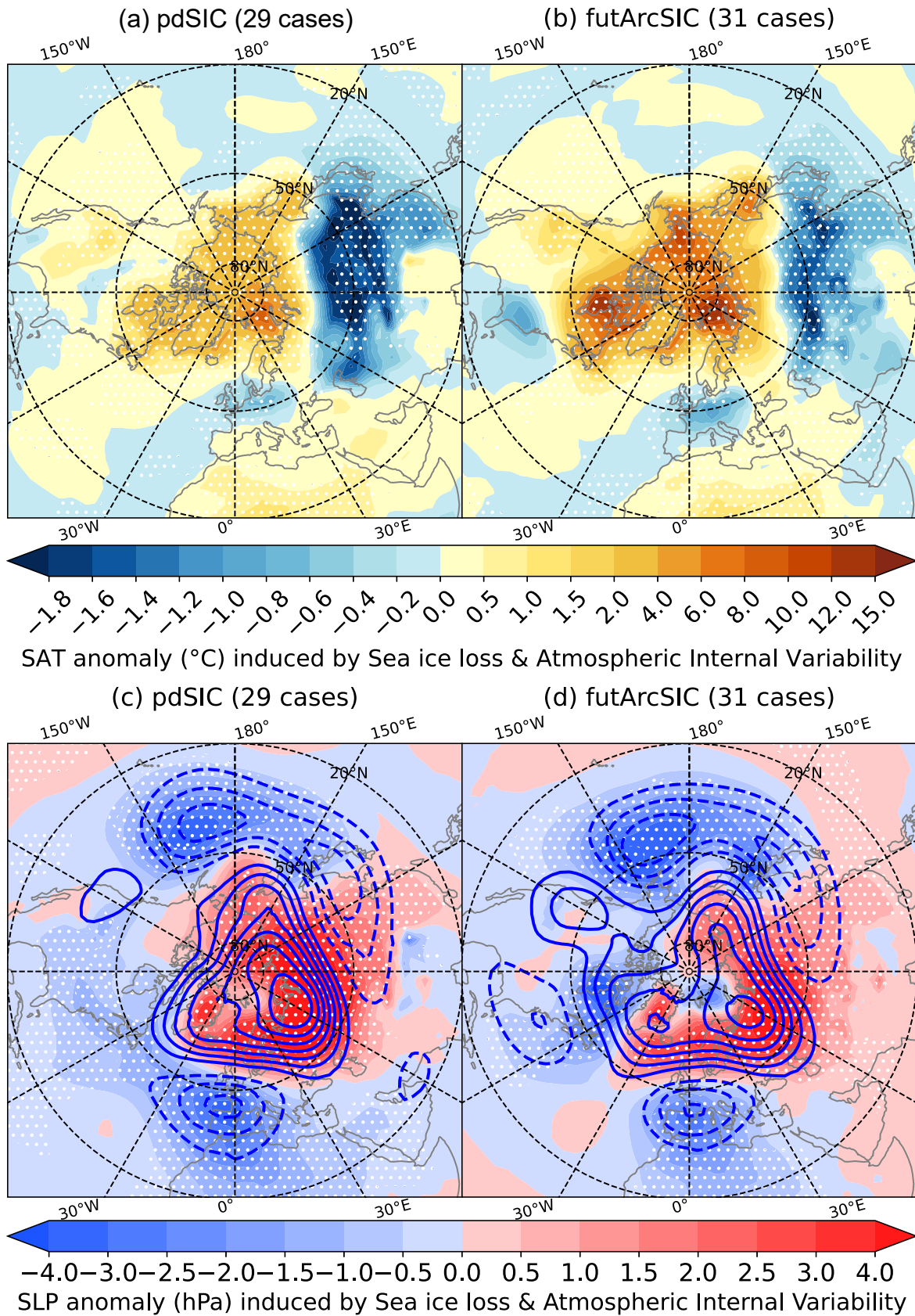


Fig. 11. The joint impact of Arctic sea ice loss and atmospheric internal variability as demonstrated by anomalies of (a, b) SAT, and (c, d) SLP (shading) and H500 (contours; interval of 10 gpm) between the ensemble mean of special members with extreme Arctic warming (red dots in Fig. 8) in pdSIC (or futArcSIC) and the ensemble mean of all members in piArcSIC. Stippling indicates the anomalies significant at the 95% confidence level.

and has stronger Ural blocking. This suggests that the observed “warm Arctic, cold East Asia” pattern (Fig. 2c) may be induced by a combination of Arctic sea ice loss and internal factors.

The standard deviation of the 200 ensemble members, which can be interpreted as a measure of atmospheric internal variability, shows a similar spatial distribution as the observation-based counterpart (Fig. 6). The contribution of atmospheric internal variability is smaller in the Arctic where sea ice loss is the dominant factor with maximum contributions of ~60% in pdSIC and ~80% in futArcSIC (Figs. 7, 8). Additionally, the Arctic sea ice loss tends to lower the East Asia winter SAT (Figs. 2a, b), but the contribution is less than 30% of the observed magnitude which is estimated by the regression onto the observed Arctic sea ice reduction (Fig. 2c).

When there are no forcing effects of sea ice loss and other external forcings (i.e., the ensemble mean was removed from each individual ensemble member), Arctic warming and East Asian cooling can be comparable in magnitude (Fig. 9). The effect of atmospheric internal variability on Arctic warming may weaken with continued sea ice loss. Such a pattern of “warm Arctic, cold East Asia” is caused by atmospheric circulation patterns which show (i) a negative phase of North Atlantic oscillation, (ii) an intensified Ural blocking, (iii) a strengthened Siberian high, and (iv) a deepened East Asian trough (Fig. 10). In summary, the Arctic sea ice loss can reinforce the “warm Arctic, cold East Asia” pattern induced by the atmospheric internal variability, and vice versa (Figs. 11a, b). If out of phase, atmospheric internal variability can easily mask out or even reverse ice-induced East Asian cooling effects since the magnitude of the internally-induced SAT variability is more than three times as large as the ice-induced variability over East Asia. It indicates that the observed “warm Arctic, cold East Asia” pattern may be a combined effect of Arctic sea ice loss and atmospheric internal variability: the former dominating the Arctic warming with the latter dominating the East Asian winter cooling.

Indeed, there are some caveats to the conclusions of this study. The simulations used in this study are lacking the oceanic dynamics and an interactive stratosphere component which play crucial roles in the observed climate variability (Marshall and Schott, 1999), and all forcing beyond sea ice is held at 2000 levels. The above conclusions can only be linked to specific observed phenomena where Arctic sea ice loss is the dominant factor over other means of internal climate variability such as El Niño-Southern Oscillation (ENSO) and ocean temperatures in the Gulf Stream, etc. ENSO can significantly influence winter air temperature variability in East Asia by modulating the strength and duration of the Ural blocking episodes (Luo et al., 2021) or modulating the intensity of the East Asian winter monsoon (He and Wang, 2013; He et al., 2013). Sato et al. (2014) revealed that a poleward shift of a sea surface temperature front over the Gulf Stream likely induces a simultaneous sea-ice decline over the Barents Sea sector and a cold anomaly over

Eurasia. Thus, the absence of dynamic and thermodynamic ocean component prevents this study from fully explaining the observed winter cooling over the Eurasian continent. Additionally, this study is based on monthly mean values. Further analysis on daily timescales may give more insight into the causality between Arctic sea ice loss and cold winter temperatures in the Eurasian continent. Nevertheless, this study has provided us with an idealistic framework where the climatic impact of Arctic sea ice, if it does exist, can be verified against the chaotic variability which is a major feature of climate in the real world. This study may give some insights into understanding future climate anomaly that is distinguished from the present day.

Acknowledgements. This research was supported by the Chinese-Norwegian Collaboration Projects within Climate Systems jointly funded by the National Key Research and Development Program of China (Grant No. 2022YFE0106800) and the Research Council of Norway funded project MAPARC (Grant No. 328943). We acknowledge the support from the Research Council of Norway funded project BASIC (Grant No. 325440) and the Horizon 2020 project APPLICATE (Grant No. 727862). High-performance computing and storage resources were performed on resources provided by Sigma2 - the National Infrastructure for High-Performance Computing and Data Storage in Norway (through projects NS8121K, NN8121K, NN2345K, NS2345K, NS9560K, NS9252K, and NS9034K).

Data Availability Statement. Forcing fields for the PAMIP experiments are available from the input4MIPs data server (<https://esgf-node.llnl.gov/search/input4mips/>). The simulations used in this study are publicly available at <https://esgf-node.llnl.gov/search/cmip6/>. A detailed description of PAMIP is available from <https://www.cesm.ucar.edu/projects/CMIP6/PAMIP/>. The Arctic sea ice extent index can be downloaded from the National Snow and Ice Data Center: https://nsidc.org/data/seaice_index. ERA5 data can be obtained from: <https://www.ecmwf.int/en/forecasts/dataset/ecmwf-reanalysis-v5>.

Code availability Scripts are available at Zenodo under the identifier <https://doi.org/10.5281/zenodo.10047912>.

Author contributions: Conceptualization – Shengping HE, Helge DRANGE; Data curation – Lise Seland GRAFF, Shengping He; Formal analysis – Shengping HE; Investigation – Shengping HE, Helge DRANGE; Methodology – Shengping HE, Helge DRANGE, Lise Seland GRAFF; Project administration – Shengping HE; Software – Shengping HE; Lise Seland GRAFF; Visualization – Shengping HE; Writing – original draft – Preparation, Shengping HE, Helge DRANGE; Writing – review & editing – Preparation, Shengping HE, Helge DRANGE, Tore FUREVIK, Huijun WANG, Ke FAN, Lise Seland GRAFF, Yvan J. ORSOLINI.

Open Access This article is licensed under a Creative Commons Attribution 4.0 International License, which permits use, sharing, adaptation, distribution and reproduction in any medium or format, as long as you give appropriate credit to the original author(s) and

the source, provide a link to the Creative Commons licence, and indicate if changes were made. The images or other third party material in this article are included in the article's Creative Commons licence, unless indicated otherwise in a credit line to the material. If material is not included in the article's Creative Commons licence and your intended use is not permitted by statutory regulation or exceeds the permitted use, you will need to obtain permission directly from the copyright holder. To view a copy of this licence, visit <http://creativecommons.org/licenses/by/4.0/>.

Funding Note: Open Access funding provided by University of Bergen (incl Haukeland University Hospital) .

REFERENCES

- Arrhenius, S., 1896: XXXI. On the influence of carbonic acid in the air upon the temperature of the ground. *The London, Edinburgh, and Dublin Philosophical Magazine and Journal of Science*, **41**, 237–276, <https://doi.org/10.1080/14786449608620846>.
- Blackport, R., and J. A. Screen, 2021: Observed statistical connections overestimate the causal effects of Arctic sea ice changes on midlatitude winter climate. *J. Climate*, **34**, 3021–3038, <https://doi.org/10.1175/JCLI-D-20-0293.1>.
- Blunden, J., and D. S. Arndt, 2012: State of the climate in 2011. *Bull. Amer. Meteor. Soc.*, **93**, S1–S282, <https://doi.org/10.1175/2012BAMSSStateoftheClimate.1>.
- Cohen, J., J. Jones, J. C. Furtado, and E. Tziperman, 2013: Warm Arctic, cold continents: A common pattern related to Arctic sea ice melt, snow advance, and extreme winter weather. *Oceanography*, **26**, 150–160, <https://doi.org/10.5670/oceanog.2013.70>.
- Cohen, J., and Coauthors, 2014: Recent Arctic amplification and extreme mid-latitude weather. *Nature Geoscience*, **7**, 627–637, <https://doi.org/10.1038/ngeo2234>.
- Cohen, J., and Coauthors, 2020: Divergent consensus on Arctic amplification influence on midlatitude severe winter weather. *Nature Climate Change*, **10**, 20–29, <https://doi.org/10.1038/s41558-019-0662-y>.
- Cohen, J. L., J. C. Furtado, M. A. Barlow, V. A. Alexeev, and J. E. Cherry, 2012: Arctic warming, increasing snow cover and widespread boreal winter cooling. *Environmental Research Letters*, **7**, 014007, <https://doi.org/10.1088/1748-9326/7/1/014007>.
- Coumou, D., G. Di Capua, S. Vavrus, L. Wang, and S. Wang, 2018: The influence of Arctic amplification on mid-latitude summer circulation. *Nature Communications*, **9**, 2959, <https://doi.org/10.1038/s41467-018-05256-8>.
- Dai, A. G., D. H. Luo, M. R. Song, and J. P. Liu, 2019: Arctic amplification is caused by sea-ice loss under increasing CO₂. *Nature Communications*, **10**, 121, <https://doi.org/10.1038/s41467-018-07954-9>.
- Danabasoglu, G., and Coauthors, 2020: The community earth system model version 2 (CESM2). *Journal of Advances in Modeling Earth Systems*, **12**, e2019MS001916, <https://doi.org/10.1029/2019MS001916>.
- England, M. R., I. Eisenman, and T. J. W. Wagner, 2022: Spurious climate impacts in coupled sea ice loss simulations. *J. Climate*, **35**, 7401–7411, <https://doi.org/10.1175/JCLI-D-21-0647.1>.
- Fetterer, F., K. Knowles, W. Meier, M. Savoie, and A. K. Windnagel, 2017, updated daily. Sea Ice Index, Version 3. [Indicate subset used]. Boulder, Colorado USA. NSIDC: National Snow and Ice Data Center. doi: <http://dx.doi.org/10.7265/N5K072F8>.
- Francis, J. A., 2017: Why are Arctic linkages to extreme weather still up in the air. *Bull. Amer. Meteor. Soc.*, **98**, 2551–2557, <https://doi.org/10.1175/BAMS-D-17-0006.1>.
- Francis, J. A., and S. J. Vavrus, 2015: Evidence for a wavier jet stream in response to rapid Arctic warming. *Environmental Research Letters*, **10**, 014005, <https://doi.org/10.1088/1748-9326/10/1/014005>.
- Francis, J. A., S. J. Vavrus, and J. Cohen, 2017: Amplified Arctic warming and mid-latitude weather: New perspectives on emerging connections. *WIREs Climate Change*, **8**, e474, <https://doi.org/10.1002/wcc.474>.
- Furevik, T., M. Bentsen, H. Drange, I. K. T. Kindem, N. G. Kvamstø, and A. Sorteberg, 2003: Description and evaluation of the bergen climate model: ARPEGE coupled with MICOM. *Climate Dyn.*, **21**, 27–51, <https://doi.org/10.1007/s00382-003-0317-5>.
- Gao, Y. Q., and Coauthors, 2015: Arctic sea ice and Eurasian climate: A review. *Adv. Atmos. Sci.*, **32**, 92–114, <https://doi.org/10.1007/s00376-014-0009-6>.
- Hasselmann, K., 1997: Multi-pattern fingerprint method for detection and attribution of climate change. *Climate Dyn.*, **13**, 601–611, <https://doi.org/10.1007/s003820050185>.
- Haustein, K., M. R. Allen, P. M. Forster, F. E. L. Otto, D. M. Mitchell, H. D. Matthews, and D. J. Frame, 2017: A real-time global warming index. *Scientific Reports*, **7**, 15417, <https://doi.org/10.1038/s41598-017-14828-5>.
- He, S. P., and H. J. Wang, 2013: Oscillating relationship between the East Asian winter monsoon and ENSO. *J. Climate*, **26**, 9819–9838, <https://doi.org/10.1175/JCLI-D-13-00174.1>.
- He, S. P., H. J. Wang, and J. P. Liu, 2013: Changes in the relationship between ENSO and Asia–Pacific midlatitude winter atmospheric circulation. *J. Climate*, **26**, 3377–3393, <https://doi.org/10.1175/JCLI-D-12-00355.1>.
- He, S. P., E. M. Knudsen, D. W. J. Thompson, and T. Furevik, 2018: Evidence for predictive skill of high-latitude climate due to midsummer sea ice extent anomalies. *Geophys. Res. Lett.*, **45**, 9114–9122, <https://doi.org/10.1029/2018GL078281>.
- He, S. P., X. P. Xu, T. Furevik, and Y. Q. Gao, 2020: Eurasian cooling linked to the vertical distribution of Arctic warming. *Geophys. Res. Lett.*, **47**, e2020GL087212, <https://doi.org/10.1029/2020GL087212>.
- Hersbach, H., B. Bell, P. Berrisford, S. Hirahara, A. Horányi, et al., 2020: The ERA5 global reanalysis. *Quarterly Journal of the Royal Meteorological Society*, **146**(730), 1999–2049.
- Honda, M., J. Inoue, and S. Yamane, 2009: Influence of low Arctic sea-ice minima on anomalously cold Eurasian winters. *Geophys. Res. Lett.*, **36**, L08707, <https://doi.org/10.1029/2008GL037079>.
- Kay, J. E., and Coauthors, 2015: The Community Earth System Model (CESM) large ensemble project: A community resource for studying climate change in the presence of internal climate variability. *Bull. Amer. Meteor. Soc.*, **96**,

- 1333–1349, <https://doi.org/10.1175/BAMS-D-13-00255.1>.
- Kim, B.-M., S.-W. Son, S.-K. Min, J.-H. Jeong, S.-J. Kim, X. D. Zhang, T. Shim, and J.-H. Yoon, 2014: Weakening of the stratospheric polar vortex by Arctic sea-ice loss. *Nature Communications*, **5**, 4646, <https://doi.org/10.1038/ncomms5646>.
- Kim, B.-M., and Coauthors, 2017: Major cause of unprecedented Arctic warming in January 2016: Critical role of an Atlantic windstorm. *Scientific Reports*, **7**, 40051, <https://doi.org/10.1038/srep40051>.
- Kug, J.-S., J.-H. Jeong, Y.-S. Jang, B.-M. Kim, C. K. Folland, S.-K. Min, and S.-W. Son, 2015: Two distinct influences of Arctic warming on cold winters over North America and East Asia. *Nature Geoscience*, **8**, 759–762, <https://doi.org/10.1038/NNGEO2517>.
- Labe, Z., Y. Peings, and G. Magnusdottir, 2020: Warm arctic, cold siberia pattern: Role of full arctic amplification versus sea ice loss alone. *Geophys. Res. Lett.*, **47**, e2020GL088583, <https://doi.org/10.1029/2020GL088583>.
- Li, F., and H. J. Wang, 2013: Relationship between Bering Sea ice cover and East Asian winter monsoon year-to-year variations. *Adv. Atmos. Sci.*, **30**, 48–56, <https://doi.org/10.1007/s00376-012-2071-2>.
- Li, F., H. J. Wang, and Y. Q. Gao, 2014: On the strengthened relationship between the East Asian winter monsoon and Arctic oscillation: A comparison of 1950–70 and 1983–2012. *J. Climate*, **27**, 5075–5091, <https://doi.org/10.1175/JCLI-D-13-00335.1>.
- Liu, J. P., J. A. Curry, H. J. Wang, M. R. Song, and R. M. Horton, 2012: Impact of declining Arctic sea ice on winter snowfall. *Proceedings of the National Academy of Sciences of the United States of America*, **109**, 4074–4079, <https://doi.org/10.1073/pnas.1114910109>.
- Luo, B. H., D. H. Luo, A. G. Dai, I. Simmonds, and L. X. Wu, 2021: A connection of winter Eurasian cold anomaly to the modulation of ural blocking by ENSO. *Geophys. Res. Lett.*, **48**, e2021GL094304, <https://doi.org/10.1029/2021GL094304>.
- Luo, D. H., Y. Q. Xiao, Y. Yao, A. G. Dai, I. Simmonds, and C. L. Franzke, 2016: Impact of ural blocking on winter warm Arctic–cold Eurasian anomalies. Part I: Blocking-induced amplification. *J. Climate*, **29**, 3925–3947, <https://doi.org/10.1175/JCLI-D-15-0611.1>.
- Ma, S. M., and C. W. Zhu, 2019: Extreme cold wave over East Asia in January 2016: A possible response to the larger internal atmospheric variability induced by Arctic warming. *J. Climate*, **32**, 1203–1216, <https://doi.org/10.1175/JCLI-D-18-0234.1>.
- Manabe, S., and R. J. Stouffer, 1980: Sensitivity of a global climate model to an increase of CO₂ concentration in the atmosphere. *J. Geophys. Res.*, **85**, 5529–5554, <https://doi.org/10.1029/JC085iC10p05529>.
- Marshall, J., and F. Schott, 1999: Open-ocean convection: Observations, theory, and models. *Rev. Geophys.*, **37**, 1–64, <https://doi.org/10.1029/98RG02739>.
- McCusker, K. E., J. C. Fyfe, and M. Sigmond, 2016: Twenty-five winters of unexpected Eurasian cooling unlikely due to Arctic sea-ice loss. *Nature Geoscience*, **9**, 838–842, <https://doi.org/10.1038/ngeo2820>.
- Mori, M., M. Watanabe, H. Shiogama, J. Inoue, and M. Kimoto, 2014: Robust Arctic sea-ice influence on the frequent Eurasian cold winters in past decades. *Nature Geoscience*, **7**, 869–873, <https://doi.org/10.1038/ngeo2277>.
- Mori, M., Y. Kosaka, M. Watanabe, H. Nakamura, and M. Kimoto, 2019: A reconciled estimate of the influence of Arctic sea-ice loss on recent Eurasian cooling. *Nature Climate Change*, **9**, 123–129, <https://doi.org/10.1038/s41558-018-0379-3>.
- Ogawa, F., and Coauthors, 2018: Evaluating impacts of recent Arctic sea ice loss on the northern hemisphere winter climate change. *Geophys. Res. Lett.*, **45**, 3255–3263, <https://doi.org/10.1002/2017GL076502>.
- Orsolini, Y. J., R. Senan, R. E. Benestad, and A. Melsom, 2012: Autumn atmospheric response to the 2007 low Arctic sea ice extent in coupled ocean–atmosphere hindcasts. *Climate Dyn.*, **38**, 2437–2448, <https://doi.org/10.1007/s00382-011-1169-z>.
- Outten, S., and Coauthors, 2023: Reconciling conflicting evidence for the cause of the observed early 21st century Eurasian cooling. *Weather and Climate Dynamics*, **4**, 95–114, <https://doi.org/10.5194/wcd-4-95-2023>.
- Outten, S. D., and I. Esau, 2012: A link between Arctic sea ice and recent cooling trends over Eurasia. *Climatic Change*, **110**, 1069–1075, <https://doi.org/10.1007/s10584-011-0334-z>.
- Peings, Y., Z. M. Labe, and G. Magnusdottir, 2021: Are 100 ensemble members enough to capture the remote atmospheric response to + 2°C Arctic sea ice loss. *J. Climate*, **34**, 3751–3769, <https://doi.org/10.1175/JCLI-D-20-0613.1>.
- Rayner, N. A., D. E. Parker, E. B. Horton, C. K. Folland, L. V. Alexander, D. P. Rowell, E. C. Kent, and A. Kaplan, 2003: Global analyses of sea surface temperature, sea ice, and night marine air temperature since the late nineteenth century. *J. Geophys. Res.*, **108**, 4407, <https://doi.org/10.1029/2002JD002670>.
- Sato, K., J. Inoue, and M. Watanabe, 2014: Influence of the Gulf Stream on the Barents Sea ice retreat and Eurasian coldness during early winter. *Environmental Research Letters*, **9**, 084009, <https://doi.org/10.1088/1748-9326/9/8/084009>.
- Screen, J. A., and I. Simmonds, 2010: The central role of diminishing sea ice in recent Arctic temperature amplification. *Nature*, **464**, 1334–1337, <https://doi.org/10.1038/nature09051>.
- Screen, J. A., I. Simmonds, C. Deser, and R. Tomas, 2013: The atmospheric response to three decades of observed Arctic sea ice loss. *J. Climate*, **26**, 1230–1248, <https://doi.org/10.1175/JCLI-D-12-00063.1>.
- Screen, J. A., and Coauthors, 2018: Consistency and discrepancy in the atmospheric response to Arctic sea-ice loss across climate models. *Nature Geoscience*, **1**, 155–163, <https://doi.org/10.1038/s41561-018-0059-y>.
- Seland, Ø., and Coauthors, 2020: Overview of the Norwegian Earth System Model (NorESM2) and key climate response of CMIP6 DECK, historical, and scenario simulations. *Geoscientific Model Development*, **13**, 6165–6200, <https://doi.org/10.5194/gmd-13-6165-2020>.
- Serreze, M. C., M. M. Holland, and J. Stroeve, 2007: Perspectives on the Arctic's shrinking sea-ice cover. *Science*, **315**, 1533–1536, <https://doi.org/10.1126/science.1139426>.
- Smith, D. M., N. J. Dunstone, A. A. Scaife, E. K. Fiedler, D. Copey, and S. C. Hardiman, 2017: Atmospheric response to

- Arctic and Antarctic sea ice: The importance of ocean–atmosphere coupling and the background state. *J. Climate*, **30**, 4547–4565, <https://doi.org/10.1175/JCLI-D-16-0564.1>.
- Smith, D. M., and Coauthors, 2019: The Polar Amplification Model Intercomparison Project (PAMIP) contribution to CMIP6: Investigating the causes and consequences of polar amplification. *Geoscientific Model Development*, **12**, 1139–1164, <https://doi.org/10.5194/gmd-12-1139-2019>.
- Smith, D. M., and Coauthors, 2022: Robust but weak winter atmospheric circulation response to future Arctic sea ice loss. *Nature Communications*, **13**, 727, <https://doi.org/10.1038/S41467-022-28283-Y>.
- Thompson, D. W. J., and J. M. Wallace, 2001: Regional climate impacts of the Northern Hemisphere annular mode. *Science*, **293**, 85–89, <https://doi.org/10.1126/science.1058958>.
- Webster, M., and Coauthors, 2018: Snow in the changing sea-ice systems. *Nature Climate Change*, **8**, 946–953, <https://doi.org/10.1038/s41558-018-0286-7>.
- Xu, X. P., S. P. He, Y. Q. Gao, T. Furevik, H. J. Wang, F. Li, and F. Ogawa, 2019: Strengthened linkage between midlatitudes and Arctic in boreal winter. *Climate Dyn.*, **53**, 3971–3983, <https://doi.org/10.1007/s00382-019-04764-7>.
- Xu, X. P., S. P. He, B. T. Zhou, and H. J. Wang, 2022a: Atmospheric contributions to the reversal of surface temperature anomalies between early and late winter over Eurasia. *Earth's Future*, **10**, e2022EF002790, <https://doi.org/10.1029/2022EF002790>.
- Xu, X. P., S. P. He, B. T. Zhou, H. J. Wang, and S. Outten, 2022b: The role of mid-latitude westerly jet in the impacts of november Ural blocking on early-winter warmer Arctic-colder Eurasia pattern. *Geophys. Res. Lett.*, **49**, e2022GL099096, <https://doi.org/10.1029/2022GL099096>.
- Zappa, G., P. Ceppi, and T. G. Shepherd, 2021: Eurasian cooling in response to Arctic sea-ice loss is not proved by maximum covariance analysis. *Nature Climate Change*, **11**, 106–108, <https://doi.org/10.1038/s41558-020-00982-8>.
- Zhang, J. R., Y. J. Orsolini, V. Limpasuvan, and J. Ukita, 2022: Impact of the Pacific sector sea ice loss on the sudden stratospheric warming characteristics. *npj Climate and Atmospheric Science*, **5**, 74, <https://doi.org/10.1038/S41612-022-00296-W>.
- Zhang, J. K., W. S. Tian, M. P. Chipperfield, F. Xie, and J. L. Huang, 2016: Persistent shift of the Arctic polar vortex towards the Eurasian continent in recent decades. *Nature Climate Change*, **6**, 1094–1099, <https://doi.org/10.1038/nclimate3136>.
- Zhang, Y. J., Z. C. Yin, H. J. Wang, and S. P. He, 2021: 2020/21 record-breaking cold waves in east of China enhanced by the ‘Warm Arctic-Cold Siberia’ pattern. *Environmental Research Letters*, **16**, 094040, <https://doi.org/10.1088/1748-9326/ac1f46>.